High Rate Capability of a Dual-Porosity $LiFePO_4$/C Composite

Nupur Nikkan Sinha,[†] C. Shivakumara,[‡] and N. Munichandraiah*[,†]

Department of Inorganic and Physical Chemistry and Solid State and Structural Chemistry Unit, Indian Institute of Science, Bangalore 560 012, India

ABSTRACT Mesoporous intercalation compounds consisting of two different distributions of pores represent a potentially attractive material for high-rate cathodes. A mesoporous $LiFePO_4$/C composite with two sizes of pores is prepared for the first time via a solution-based polymer templating technique. The precursor of the $LiFePO_4$/C composite is heated at different temperatures in the range from 600 to 800 °C to study the effect of crystallinity, porosity, and morphology on the electrochemical performance. The composite is found to attain reduction in the surface area, carbon content, and porosity upon increasing temperature. Nonetheless, the composite prepared at 700 °C with pore-size distributions of around 4 and 50 nm exhibits a high rate capability and stable capacity retention upon cycling.

KEYWORDS: cathode material • Li-ion battery • mesoprous material • high rate capability

INTRODUCTION

A rechargeable Li-ion battery is the state-of-the art power source for portable electronic devices such as wireless phones, laptop computers, camcorders, etc. Presently, this battery system is under development for electric vehicle application because of its high energy density and long cycle life (1, 2). Since commercialization of the Li-ion cell using $LiCoO_2$ as the cathode material by Sony in 1991, alternate cathode materials have been investigated to improve the cell performance, decrease the cost, and increase the safety. Among several cathode materials, olivine $LiFePO_4$ is found to be attractive because of its low cost, environmental compatibility, cycling stability, high thermal stability, and safety (3–6). The strong covalency in PO_4 stabilizes the antibonding Fe^{3+}/Fe^{2+} state through an Fe−O−P inductive effect, which restricts the extraction of oxygen compared with other cathode materials such $LiCoO_2$, $LiNiO_2$, and $LiMn_2O_4$ (3). In recent years, nanostructured porous materials have been considered as promising materials for application in the field of rechargeable Li-ion batteries because of their sustainable advantages in fast mass and charge transport (7–9). Porous materials provide short solid-state diffusion paths and efficient access of the electrolyte into the pores, which hasten the ionic supply. However, pores with diameters of less than 2 nm get blocked by trapped ions, and hence these pores are no longer active for electrolyte transport (10). As a consequence, the capacity of the material decreases. The material with a suitable distribution of both small (2−5 nm) and large (30−50 nm) pores can provide easy access of ions to the bulk of the electrode, where larger pores favor the mass transport of solvated ions into the smaller pores and thus reduce the transport limitation (11). Therefore, maintaining a distribution of dual pores in mesoporous materials can potentially improve the charge transport and rate capability of the material.

Several methods, such as colloid crystal templating, dual templating of surfactants, and so on, have been reported for the synthesis of porous materials (11–13). Nanocasting of hard templates is an effective method of preparing hierarchically porous compounds (12). However, $LiFePO_4$ cannot be prepared directly by hard templates such as carbon and silica monolith because $LiFePO_4$ dissolves during removal of the template by reaction with HF or NaOH (12). In the case of a $LiFePO_4$/C composite, $LiFePO_4$ gets oxidized during removal of the carbon template in the presence of oxygen (12). Lim et al. (14) reported the synthesis of a hollow $LiFePO_4$ material by the hard-template route. However, the presence of silicon and sodium as impurities along with $LiFePO_4$ was reported. Triblock polymers (F127 and F108) were added into the precursor solutions so as to provide a thin carbon coating around the $LiFePO_4$ particles and also to improve penetration of the precursor solutions into the carbon monolith (12). Until now, only one group (13) reported the synthesis of hierarchically porous $LiFePO_4$ by solution-based templating methods, using poly(methyl methacrylate) (PMMA) colloids as templates. There are no other reports, to the best of the authors' knowledge, on the synthesis of dual-porosity $LiFePO_4$ by a solution-based templating method.

In the present study, a hierarchically porous $LiFePO_4$/C composite is synthesized for the first time by a solution-based templating technique, using pluronic acid [P123: poly(EO)$_{\sim}$-*block*-poly(PO)$_{\sim}$-*block*-poly(EO) triblock polymer, where EO = ethylene glycol and PO = propylene glycol] as the templating agent in the presence of a cosurfactant (*n*-

* To whom correspondence should be addressed. E-mail: muni@ipc.iisc.ernet.in. Tel: +91-80-22933183. Fax: +91-80-2360-0683.
Received for review April 5, 2010 and accepted June 22, 2010
[†] Department of Inorganic and Physical Chemistry.
[‡] Solid State and Structural Chemistry Unit.
DOI: 10.1021/am100309w

butanol) in an emulsion medium. The $LiFePO_4$/C composite possesses two kinds of pores. The results show that the porous $LiFePO_4$/C composite prepared at 700 °C can deliver a high discharge capacity with high rate capability.

EXPERIMENTAL SECTION

Analytical-grade chemicals, namely, lithium nitrate (Aldrich), ferric nitrate (SD Fine Chemicals), ammonium dihydrogen phosphate (SD Fine Chemicals), cyclohexane (Merck), *n*-butanol (SD Fine Chemicals), P123 (Aldrich), 0.38-mm-thick lithium foil (Aldrich), poly(vinylidene fluoride) (PVDF; Aldrich), acetylene black (AB; Alfa Aesar), 1-methyl-2-pyrrolidinone (NMP; Aldrich), ethylene carbonate (EC; Aldrich), dimethyl carbonate (DMC; Aldrich) and $LiAsF_6$ (Aldrich), were used as received. Aqueous solutions of metal nitrates and ammonium dihydrogen phosphate were prepared using doubly distilled water. In a typical synthesis, polymer template P123 (1.0 g) was dissolved in a mixed solution consisting of 51.2 mL of cyclohexane (oil) and 6.2 mL of *n*-butanol (cosurfactant) and stirred well for 2 h. To this nonaqueous medium was added an aqueous solution of 15 mL consisting of 1.280 g of $Fe(NO_3)_3$, 0.218 g of $LiNO_3$, and 0.418 g of $(NH_4)H_2PO_4$ (stoichiometric amounts). The solution was stirred for 12 h to ensure homogeneity. The solution slowly turned opaque, and finally a milky white colloidal solution formed. The colloidal solution was heated at 150 °C for 2 h to evaporate the solvent and then heated at 300 °C for 4 h in a nitrogen atmosphere to get the precursor. The quantity of precursor obtained in a typical batch of the synthesis was about 0.85 g. Subsequently, the precursor samples were heated at different temperatures in the range 600−800 °C under a nitrogen atmosphere for 6 h to get the final product samples.

For electrochemical characterization, electrodes were prepared on aluminum foil (0.2 mm thick) as a current collector. A circular aluminum foil of area 1 cm^2 was polished with successive grades of emery, cleaned with detergent, etched in dilute HNO_3, washed with doubly distilled water, rinsed with acetone, dried, and weighed. The $LiFePO_4$/C composite (80 wt %), AB (15 wt %), and PVDF (5 wt %) were ground in a mortor, and a few drops of NMP were added to form a syrup. The syrup was applied by a brush onto the pretreated aluminum foil and dried at 110 °C for a few minutes. The coating and drying steps were repeated to get the required loading level (4−6 mg cm^{-2}) of the active material. The electrodes were dried at 110 °C under vacuum for 12 h. Finally the electrodes were pressed at a pressure of 25 kN by a hydraulic press. Electrochemical cells were assembled in homemade Swagelok-type poly(tetrafluoroethylene) cell holders, using a lithium foil as both the counter and reference electrodes. A glass mat soaked in the electrolyte was used as the separator. The electrolyte was 1 M $LiAsF_6$ in a 1:1 mixed solvent of EC and DMC. The solvent was repeatedly treated with molecular sieves (4 Å) before preparation of the electrolyte. Cells were assembled in an argon-atmosphere glovebox (MBraun model UNILAB).

Powder X-ray diffraction (XRD) patterns were recorded using a Bruker AXS D8 diffractometer using Cu Kα ($\lambda = 1.5418$ Å) as the source. Thermogravimetric analysis (TGA) data were recorded in the temperature range from ambient to 900 °C at a heating rate of 10 °C min^{-1} in air using a Perkin-Elmer thermal analyzer model Pyris Diamond TG/DTA. Microstructures were examined by a FEI Co. scanning electron microscope model SIRION and a high-resolution transmission electron microscope (HRTEM) model TECNAI F30. Brunauer−Emmett−Teller (BET) surface area measurements of the samples were carried out using a Micromeritics surface area analyzer model ASAP 2020. Analysis for carbon was carried out in a ThermoFinnigan FLASH EA 1112 CHNS analyzer. X-ray photoelectron spectroscopy (XPS) was carried out with a SPECS photoelectron spectrometer (Phoibos 100 MCD energy analyzer) using monochromatic Mg Kα radiation (1253.6 eV). Cyclic voltammograms were recorded with a Biologic SA multichannel potentiostat/galvanostat model VMP3. The charge−discharge cycling studies of the cells were carried out using a Bitrode battery cycle-life tester. The ambient-temperature experiments were carried out at 20 ± 1 °C in an air-conditioned room. Reproducibility of the electrochemical data was ensured by repeating the experiments with at least another electrode of the same sample. Only representative results are presented.

RESULTS AND DISCUSSION

Mesoporous inorganic oxide-based materials are synthesized by self-assembled molecular agregates or supramolecular assemblies generally employed as the structure-directing agents (15, 16). The overall process involves the formation of a precursor combined with the template from the reactants, followed by formation of the product and finally removal of the template. In the present study, a small volume of an aqueous solution consisting of $LiNO_3$, $Fe(NO_3)_3$, and $(NH_4)_2HPO_4$ was added to a large volume of cyclohexane and butanol with dissolved triblock copolymer P123. Under the reaction conditions, materials are assembled into the form of micelles, which restrict the growth of the product. Furthermore, the product species react on the surface of the polymer chain as driven by interaction between the functional groups. The addition of butanol favors the expansion of the micelle, which increases the pore size of the material. When the solution was heated at 150 °C for 2 h under a nitrogen atmosphere, the solvents were evaporated and a gel was formed. The mesoporous structure of the material was obtained by heating at 300 °C for 4 h, owing to decomposition of the polymer. However, the heating temperature plays a critical role in the decision of the porous nature of the material (17). It is known that the electrochemical performance of the cathode materials depends on the crystallinity (18), composition (19), particle size (19), morphology (20), and porosity (21), etc. In view of tailoring of the reaction product for optimum electrochemical and mesoporous properties, the precursor was subjected to further heating at different temperatures ranging from 600 to 800 °C to get the final product samples.

The precursor was subjected to TGA under a nitrogen atmosphere, and the data are presented in Figure 1. There is about 2% weight loss when the sample is heated to 100 °C, and this loss corresponds to the removal of adsorbed water. There is a continuous loss of weight with an increase in the temperature up to 500 °C. This is due to decomposition of nitrates and the polymer. It is seen that there is about 9% weight loss up to 500 °C and thereafter the mass remains unaltered up to the 900 °C, indicating the formation of product even at 500 °C, as is also evidenced by the XRD studies.

Figure 2 shows XRD patterns of the product samples obtained by heating the precursor at different temperatures for 6 h in a nitrogen atmosphere. Because the samples were heated in an inert atmosphere to prevent oxidation of iron, a significant amount of carbon residue was left in the sample, which is evidently reflected in the CHN analysis (Table 1). However, no impurity peak corresponding to

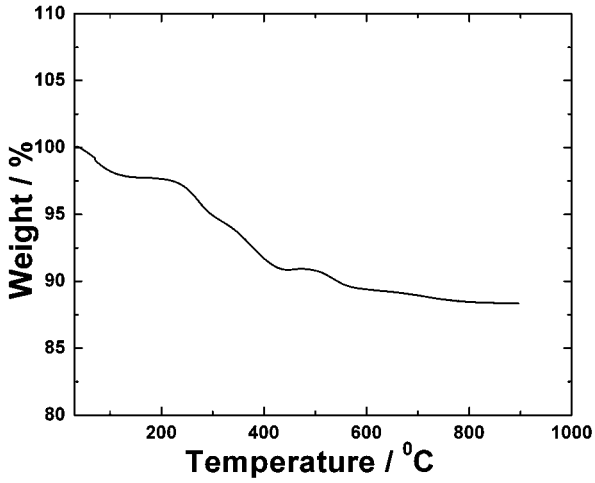

FIGURE 1. TGA curve of the precursor prepared by the polymer template route, recorded at a heating rate of 10 °C min^{-1}.

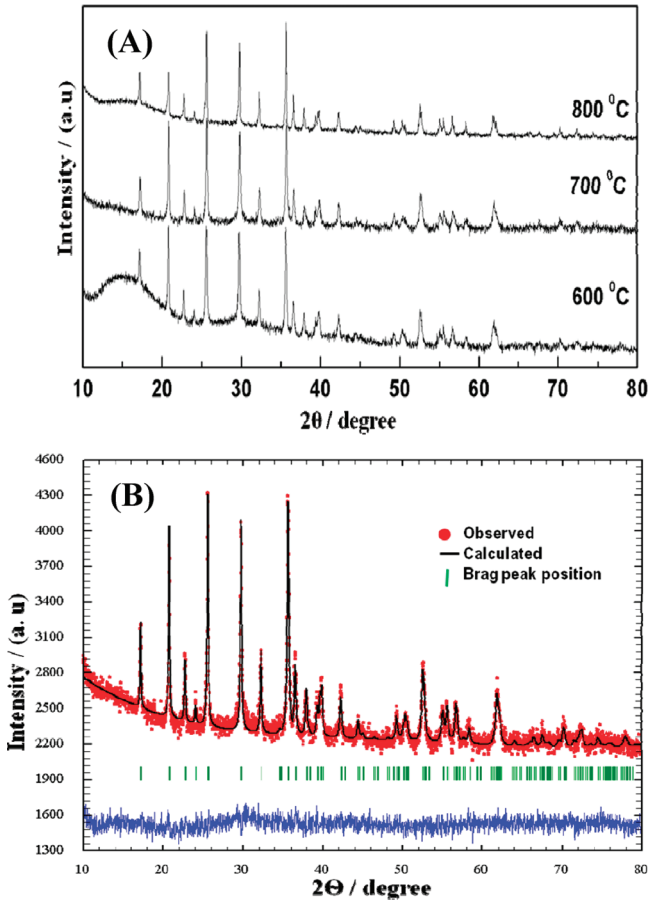

FIGURE 2. (A) Powder XRD patterns of $LiFePO_4$/C composite samples prepared at different temperatures. (B) Reitveld analysis of the $LiFePO_4$/C composite prepared at 700 °C. The bottom curve in part B indicates the error level between the experimental and fit data.

carbon is observed in XRD patterns of the samples. The patterns of all samples show the formation of a pure $LiFePO_4$ phase, and they agree well with the JCPDF file no. 40-1499. Figure 2B shows a typical Rietveld refinement result of the $LiFePO_4$/C composite material prepared at 700 °C, and all of the peaks are indexed on the basis of an orthorhombic olivine structure with a *Pnma* space group. The lattice parameters of the sample are $a = 10.328$ Å, $b = 6.008$ Å, and $c = 4.703$ Å. These values are in good agreement with those reported previously in the literature (22). The carbon content was found to decrease from 5.15% to 1.85% with an increase in the preparation temperature from 600 to 800 °C (Table 1).

Table 1. Surface Area and Carbon Content Present in the $LiFePO_4$/C Composite Prepared at Different Temperatures

heating temperature (°C)	carbon content (wt %)	surface area (m^2 g^{-1})
600	5.15	61
700	3.82	54
800	1.85	42

SEM micrographs of $LiFePO_4$/C composite samples prepared at different temperatures are shown in Figure 3. A porous morphology is observed for the sample prepared at 600 °C (Figure 3A). It is seen that the sample prepared at 700 °C also shows a porous structure (Figure 3B). Upon heating of the precursor at 800 °C, there is a change in the morphology. The formation of large particles of diameter 200−250 nm with a porous network of carbon atoms is observed (Figure 3C). TEM micrographs of the sample heated at 700 °C are shown in Figure 4. The formation of a porous framework with different sizes of pores is clearly seen, which is further conformed by nitrogen adsorption/desorption studies.

Nitrogen adsorption/desorption isotherms and Barrett−Joyner−Halenda (BJH) pore-size distribution curves recorded at 77 K for the $LiFePO_4$/C composites prepared at different temperatures are presented in Figure 5. Hysterisis at relative pressure p/p_0 ranging from 0.6 to 0.8, which is a characteristic feature of mesoporous materials with a type iv isotherm, is recorded for each sample (Figure 5A). The appearance of hysteresis in the isotherm is usually associated with capillary condensation in the mesopores. The BET surface area values were calculated from the adsorption isotherm in the p/p_0 range between 0.1 and 0.28 (Table 1). There is a decrease in the surface area of the $LiFePO_4$/C composite from 61 to 42 m^2 g^{-1} with an increase in the temperature due to agglomeration of the particles and also due to an increase in the particle size, as seen in SEM micrographs (Figure 3). As the samples were heated in a nitrogen atmosphere, carbon residue was left in the sample, which also contributed to the surface area. A decrease in the carbon content with temperature (Table 1) is also likely to account for the reduction in the surface area. Porosity characteristics are more evidently observed from BJH curves (Figure 5B), which reflect the presence of pores of two different sizes. For the sample, prepared at 600 °C, there is a very narrow pore-size distribution at 4 nm and a broad distribution of pores around 50 nm (Figure 5B, curve i). This kind of dual porosity in the mesoporosity range appears to have developed because of the presence of the polymer template P123 in the reaction medium used for preparation of the LiFePO4/C composite. It was found that the dual porosity did not develop when the synthesis was carried out in the absence of P123, but only a single porosity with a broad distribution

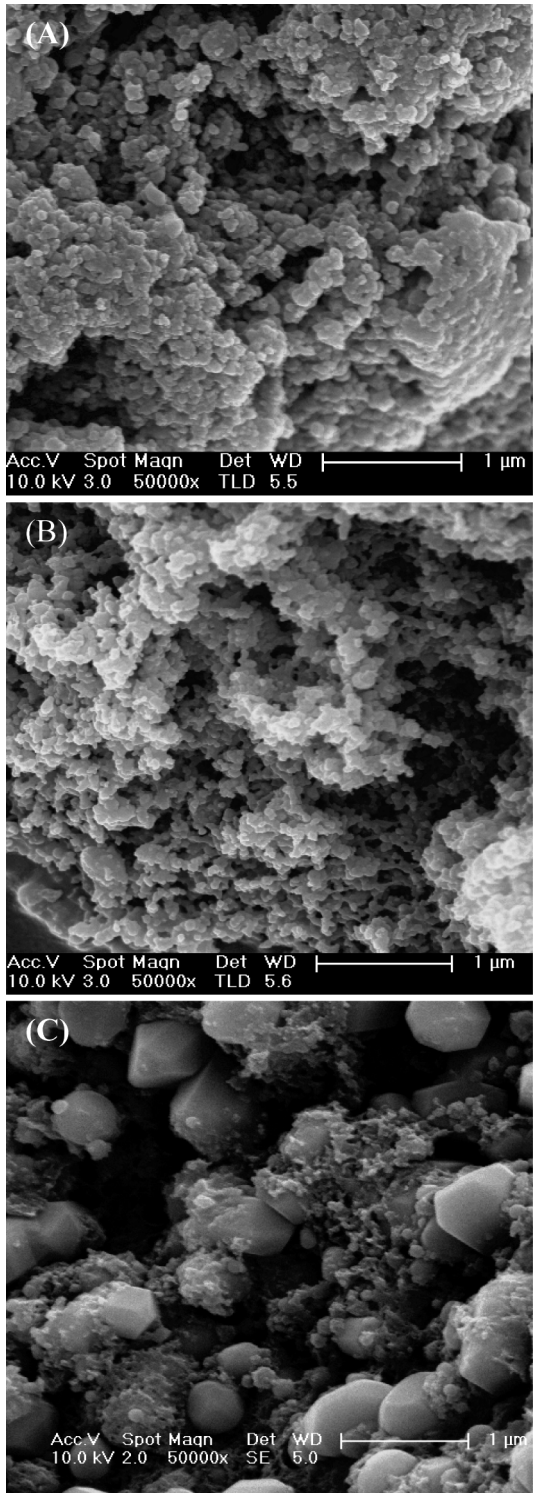

FIGURE 3. SEM images of $LiFePO_4$/C composite samples prepared at (A) 600, (B) 700, and (C) 800 °C.

of around 30 nm was observed. Upon an increase in the preparation temperature to 700 °C, the 4 nm pore-size distribution remains nearly the same as that for the 600 °C sample, but the pore volume corresponding to 50 nm pores decreases (Figure 5B, curve ii). For the sample prepared at 800 °C, the 4 nm pore-size distribution remains unaltered, but the distribution of 50 nm pores is affected significantly (Figure 5B, curve iii). The pore diameter decreases from 50 nm to about 15 nm with a significant decrease in the pore

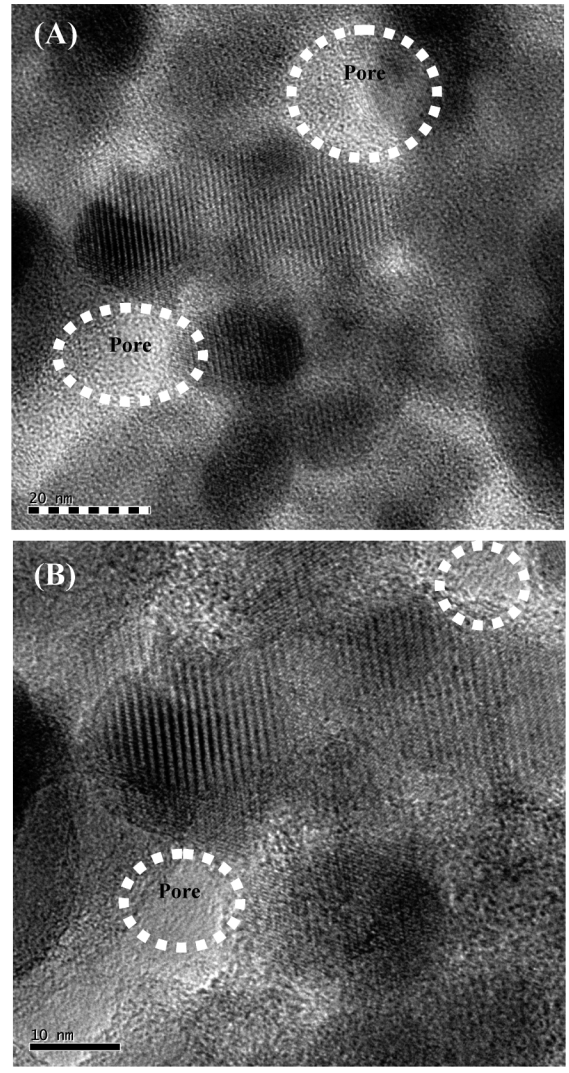

FIGURE 4. TEM images of the $LiFePO_4$/C composite prepared at 700 °C.

volume. Thus, $LiFePO_4$/C composite samples possess dual porosity, and the larger pores gradually collapse upon an increase in the preparation temperature. Similar to these data, dual-porosity pore-size distributions were reported for mesoporous MnO_2 and $LiMn_2O_4$ (17, 23). In our previous study (24), it was observed that the small pores were present up to 900 °C.

The core-level XPS spectra of Li 1s, Fe 2p, P 2p, O 1s, and C 1s for the $LiFePO_4$/C composite sample prepared at 700 °C are shown in Figure 6. In the Li 1s spectrum (Figure 6A), the symmetrical peak at a binding energy (BE) of 55.85 eV is in good agreement with the reported values for $LiFePO_4$ and layered cathode materials (25). As shown in Figure 6B, the Fe 2p spectrum splits into $2p_{1/2}$ and $2p_{3/2}$ because of spin−orbit coupling. Each part consists of a main peak and a corresponding satellite peak at BEs of 715 and 729 eV for Fe $2p_{3/2}$ and Fe $2p_{1/2}$, respectively. P 2p can be deconvoluted into two components: $2p_{3/2}$ and $2p_{1/2}$ at BEs of 133.4 and 134.3 eV, respectively. Moreover, the presence of only one doublet reveals the only environment of phosphorus, which is in good agreement with the PO_4^{3-} group. This further excluded the formation of impurity phases such as Fe_2P,

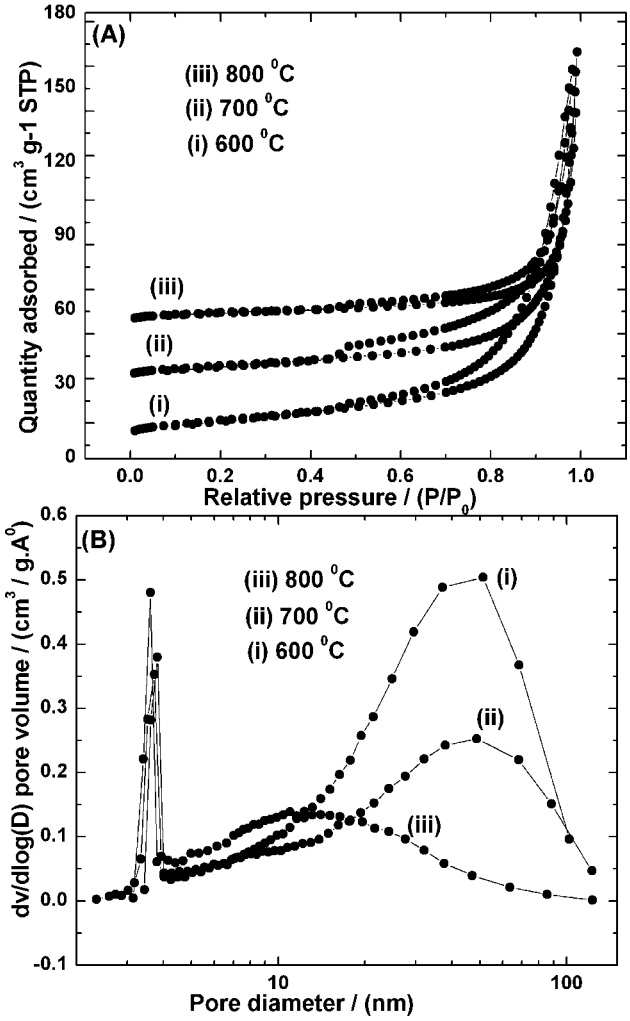

FIGURE 5. (A) Nitrogen adsorption−desorption isotherms and (B) pore-size distribution (BJH curves) of $LiFePO_4$/C composite samples prepared at different temperatures. The scale on the *Y* axis of part A is shifted up by 30 units for curve ii and by 60 units for curve iii.

which appears at a BE value of 129.5 eV (25). The C 1s spectrum can be deconvoluted into three peaks at BE values of 284.6, 285.8, and 286.5 eV, corresponding to sp^2 and sp^3 C−C bonds (24), respectively. The peak around 286.6 eV is assigned to the satellite peak of sp^2 C−C bonds (26) and C−O contamination formed at the surface because of air exposure (25). The BE values obtained here are consistent with the literature report (25).

Figure 7 shows cyclic voltammograms of $LiFePO_4$/C composite samples prepared at different temperatures in the potential range between 2.50 and 4.20 V. A pair of anodic and cathodic peaks, which correspond to a Fe^{2+}/Fe^{3+} redox couple, is observed for all of the samples. Nevertheless, the current peaks of the 700 °C sample are sharper and greater in magnitude, suggesting a better performance of this sample than the rest of the samples. Figure 8 shows the discharge profiles for $LiFePO_4$/C composite samples prepared at different temperatures in potential limits between 2.00 and 4.20 V at 0.18 C rates. The discharge capacity values obtained are 133, 156, and 139 mAh g^{-1} for 600, 700, and 800 °C samples, respectively. It is seen that the nature of the discharge profile depends on the preparation temperature. There is a sharp fall of the potential from 4.20 V to about 3.36 V upon commencement of discharge for all samples. This is due to the inherent poor electronic conductivity of $LiFePO_4$. A fairly flat discharge plateau is present during the initial stages of discharge in all curves in Figure 8. However, the time of flat discharge depends on the preparation temperature. For the sample prepared at 700 °C, the flat plateau (Figure 8, curve ii) is the longest. For the samples prepared at 600 and 700 °C (Figure 8, curves i and ii), the discharge appears to take place in two stages: the flat plateau around 3.36 V and then a sloping region up to the end of discharge. For the 800 °C sample (Figure 8, curve iii), which exhibits a faster fall of the voltage in relation to the other samples (Figure 8, curves i and ii), the majority of the discharge capacity (75%) is obtained from the plateau region and the remaining capacity (25%) is obtained from the sloping part. For the 700 °C sample, on the other hand, 64% of the discharge capacity is obtained from the flat plateau and 36% is obtained from the sloping region. The capacity contributions are 45% and 65%, respectively, from the flat and sloping regions for the 600 °C sample. It is known (27–31) that the plateau represents a two-phase reaction with the $FePO_4$ and $LiFePO_4$ phases coexisting during the Li^+-ion insertion. However, the sloping part is considered as a capacitance property because of the surface storage of lithium (28). It is well-known that a lithium-ion intercalation reaction is responsible for the discharge capacity of $LiFePO_4$. However, as the size of the particle is reduced to nanoscale, the pseudocapacitive effect, i.e., the faradaic charge storage at the surface of the material, has to be considered for the total discharge capacity of the material (29). Recently, Xia et al. (27) have shown a pseudocapacitive effect in the high-surface-area mesoporous $LiMn_2O_4$. In another study, Yang et al. (30) have reported that hierarchically constructed nanoplates of $LiFePO_4$ exhibit pseudocapacitive behavior. The presence of a pseudocapacitive effect has been observed in nanostructured TiO_2 (31). In the present study, the sloping part of the discharge curve is assigned to the pseudocapacitance behavior of nanoparticles, which is dominant for 600 and 700 °C samples. The sloping part is less for the 800 °C sample because of the increased particle size (Figure 3C) and perhaps also because of the decreased carbon content (Table 1). Wu et al. (32) reported a discharge capacity of 145 mAh g^{-1} at 0.9 C rate and a sluggish discharge slope similar to that observed in the present study. In another study, a discharge capacity of 160 mAh g^{-1} at 0.1 C rate was obtained for the hierarchically porous $LiFePO_4$/C composite prepared by using PMMA colloidal crystals as templates (13). Recently, a discharge capacity of 140 mAh g^{-1} at 0.1 C rate was reported for the $LiFePO_4$/C composite by Drummond et al. (12) Yang et al. (30) reported a discharge capacity of 100 mAh g^{-1} at 0.03 C rate for hierarchically constructed nanoplates of $LiFePO_4$ with a sloped discharge. In the present study, a good electrochemical performance of the $LiFePO_4$/C composite prepared at 700 °C is attributed to an optimized porosity.

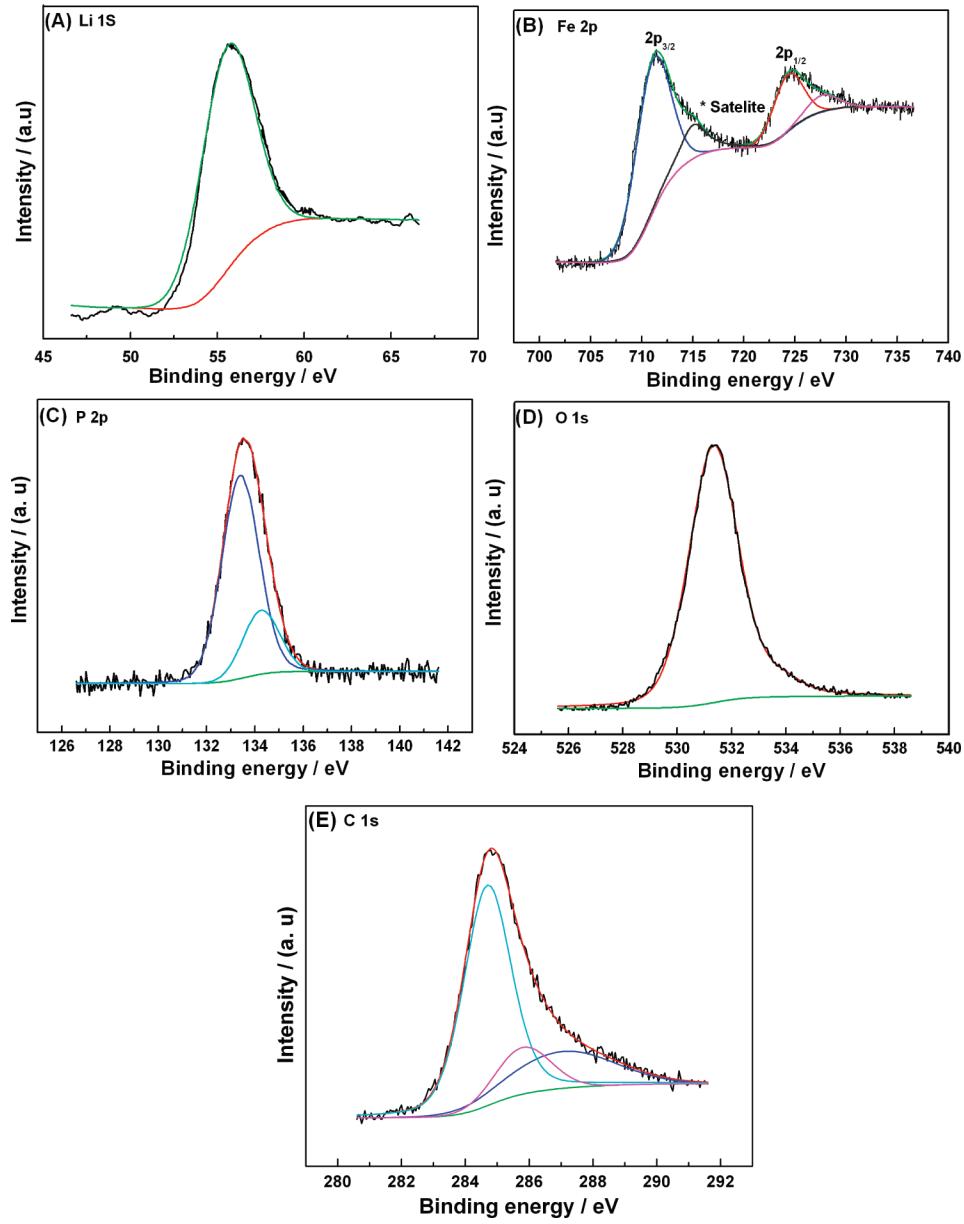

FIGURE 6. XPS spectra of Li 1s, Fe 2p, P 2p, and O 1s of the $LiFePO_4$/C composite sample prepared at 700 °C.

Figure 9 shows the discharge capacities of mesoporous $LiFePO_4$/C composites with an increase in the rate of cycling from 0.18 to 14.7 C. It is seen that the 700 °C prepared sample shows a better performance at all rates delivering discharge capacities of 156 and 56 mAh g^{-1} at 0.18 and 14.7 C rates, respectively. For 600 and 800 °C samples, the maximum rate that could be studied is 4.1 C. At 4.1 C rate, the discharge capacity values of 52 and 43 mAh g^{-1} are calculated for 600 and 800 °C samples, respectively. On the other hand, about 60 mAh g^{-1} is obtained at 14.7 C rate for the 700 °C sample. Recently, Drummond et al. (12) reported a discharge capacity of 138 mAh g^{-1} at 0.1 C rate and 110 mAh g^{-1} at 5 C rate for the $LiFePO_4$/C composite material. In another report by the same group, discharge capacities of 160 and 124 mAh g^{-1} were reported at 0.1 and 5 C rates, respectively, for the hierarchically porous $LiFePO_4$/C composite material (13). An improved performance of hollow

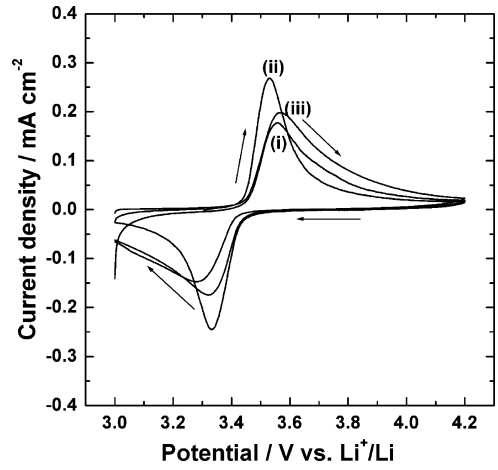

FIGURE 7. Cyclic voltammograms of $LiFePO_4$/C composite samples prepared at 600 (i), 700 (ii), and 800 °C (iii) at a sweep rate of 0.05 mV s^{-1}. Mass of the active material: 4−6 mg/cm^{-2}.

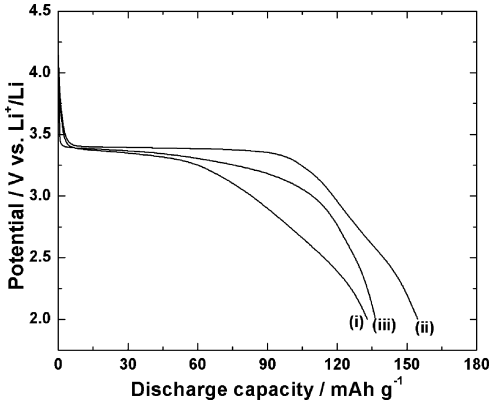

FIGURE 8. Discharge profiles of $LiFePO_4$/C composite samples prepared at 600 (i), 800 (ii), and 700 °C (iii) at 0.18 C rate. Mass of the active material: 4−6 mg/cm^{-2}.

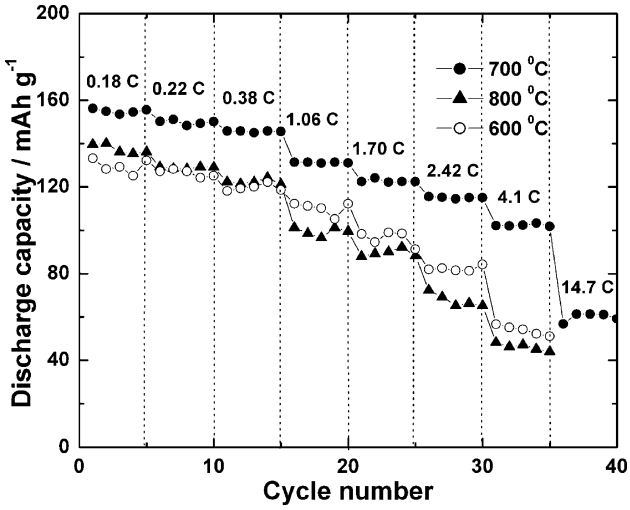

FIGURE 9. Rate capability of $LiFePO_4$/C composite samples prepared at different temperatures. Mass of the active material: 4−6 mg/cm^{-2}.

$LiFePO_4$ was reported by Lim et al. (14) Discharge capacities of 157 and 137 mAh g^{-1} were obtained at 0.2 and 15 C rates, respectively. The improved performance of the hollow $LiFePO_4$ was because of the high surface area (103 m^2 g^{-1}) of the sample. Lu et al. (33) prepared $LiFePO_4$ by PMMA bead templates and obtained discharge capacities of 145 and 100 mAh g^{-1} at 1 and 5.9 C rates. In the present study, the high rate performance of the 700 °C heated sample is attributed to the presence of dual porous structures, which are interconnected to provide efficient ionic transport.

The $LiFePO_4$/C composite samples prepared at different temperatures were subjected to a cycle-life test at 0.22 C rate between 2.0 and 4.2 V. The discharge capacity values calculated for 50 continuous charge−discharge cycles are presented in Figure 10. Stable discharge capacities of 130 and 122 mAh g^{-1} are obtained for 600 and 800 °C samples, respectively. On the other hand, the 700 °C sample delivered a higher stable discharge capacity at 150 mAh g^{-1}. Zhao et al. (34) reported a discharge capacity of 138 mAh g^{-1} at 0.1 C rate after 30 cycles for $LiFePO_4$/C. A discharge capacity of 110 mAh g^{-1} was obtained after 70 cycles at C/30 rate for hierarchically constructed nanoplates of $LiFePO_4$. In the

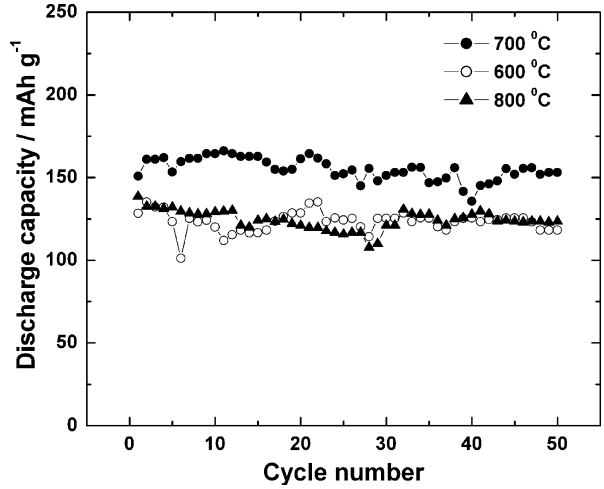

FIGURE 10. Variation of the discharge capacity of $LiFePO_4$/C composite samples prepared at different temperatures with a cycle number at C/5 rate.

present work, the 700 °C heated sample shows good capacity retention and is superior to the rest of the samples.

Generally, it is believed that the electrochemical performance of a cathode material is governed by various properties such as the surface area, morphology, carbon content, crystallinity, porosity, etc., which are influenced by the preparation temperature. An examination of the physicochemical data of LiFePO4/C composite samples prepared in the present study indicates that the crystallinity is only marginally affected by the temperature. XRD patterns (Figure 2) suggest that all samples are crystalline, but the noise level decreases with an increase of the temperature. If the crystallinity is the only parameter, which can strongly influence the electrochemical properties, the 800 °C sample with the highest crystallinity is expected to be the best composite. The fact that the 700 °C sample exhibits the best electrochemical properties suggests that high crystallinity is not essential in the present study. The SEM micrographs indicate that the 800 °C sample consists of larger particles, which are not favorable for the electrochemical properties, than the porous 700 and 600 °C samples. The surface area as well as carbon content decrease with an increase in the temperature of preparation (Table 1). These properties do not throw light on the better electrochemical performance of the 700 °C sample than the other samples. Nevertheless, the BJH data (Figure 5B) clearly indicate that the porosity at 50 nm is greatly influenced by the preparation temperature, while the porosity at 4 nm is only slightly affected. The pore volume at 50 nm is large for the 600 °C sample, and it decreases for the 700 °C sample. On the other hand, the porosity at 50 nm disappears for the 800 °C sample, and a broad distribution of 15 nm pores with low pore volume is present. Thus, the suitable dual porosity is concluded to be the appropriate factor for the better electrochemical performance of the $LiFePO_4$/C composite prepared at 700 °C than the rest of the samples. A suitable combination of the large and small pores is expected to provide an efficient electrolyte transport for the high rate capability and stable discharge

capacity of the $LiFePO_4$/C composite as the cathode material of a Li-ion cell.

CONCLUSIONS

A mesoporous $LiFePO_4$/C composite with dual porosity is prepared for the first time via a solution-based polymer templating technique. The precursor of the $LiFePO_4$/C composite is heated at different temperatures in the range from 600 to 800 °C to study the effect of the crystallinity, porosity, and morphology on the electrochemical performance. The composite is found to attain reduction in the surface area, carbon content, and porosity upon increasing temperature. Nonetheless, the composite prepared at 700 °C contains dual porosity with pore-size distributions spread around 4 and 50 nm. This composite exhibits a high rate capability and stable capacity retention upon cycling.

REFERENCES AND NOTES

(1) Nazri, A.; Pistoia, G. *Lithium Batteries: Science and Technology*; Kluwer: Boston, 2004; p 1.
(2) Goodenough., J. B.; Kim, Y. *Chem. Mater.* **2010**, *22*, 587.
(3) Padhi, A. K.; Nanjundaswamy, K. S.; Goodenough, J. B. *J. Electrochem. Soc.* **1997**, *144*, 1188.
(4) Padhi, A. K.; Nanjundaswamy, K. S.; Masquelier, C.; Okada, S.; Goodenough, J. B. *J. Electrochem. Soc.* **1997**, *144*, 1609.
(5) Yamada, A.; Cheng, S. C.; Hinokuma, K. *J. Electrochem. Soc.* **2001**, *148*, A224.
(6) MacNeil, D. D.; Lu, Z.; Chen, Z.; Dahn, J. R. *J. Power Sources* **2002**, *108*, 8.
(7) Long, J. W.; Dunn, B.; Rolison, D. R.; White, H. S. *Chem. Rev.* **2004**, *104*, 4463.
(8) Attard, G. S.; Elliot, J. M.; Bartllet, P. N.; Whitehead, A.; Owen, J. R. *Macromol. Symp.* **2000**, *156*, 179.
(9) Bruce, P. G. *Solid State Ionics* **2008**, *179*, 752.
(10) Wang, Z. Y.; Li, F.; Ergang, N. S.; Stein, A. *Chem. Mater.* **2006**, *18*, 5543.
(11) Hu, Y. S.; Adelhelm, P.; Smarsly, B. M.; Hore, S.; Antonitti, M.; Maier, J. *Adv. Funct. Mater.* **2007**, *17*, 1873.
(12) Dohetry, C. M.; Caruso, R. A.; Smarsly, B. M.; Adellhelm, P.; Drummond, C. J. *Chem. Mater.* **2009**, *21*, 5300.
(13) Dohetry, C. M.; Caruso, R. A.; Smarsly, B. M.; Drummond, C. J. *Chem. Mater.* **2009**, *21*, 2895.
(14) Lim, S.; Yoon, C. S.; Cho, J. *Chem. Mater.* **2008**, *20*, 4560.
(15) Cheng, F.; Tao, Z.; Liang, J.; Chen, J. *Chem. Mater.* **2008**, *20*, 667.
(16) Yue, W.; Zhou, W. *Prog. Nat. Sci.* **2008**, *18*, 1329.
(17) Pen, Y.; Jiao, F.; Bruce, P. G. *Microporous Mesoporous Mater.* **2009**, *121*, 90.
(18) Akimoto, J.; Gotoh, Y.; Oosawa, Y. *J. Solid State Chem.* **1998**, *141*, 298.
(19) Sheu, S. P.; Yao, C. Y.; Chen, J. M.; Shiu, Y. C. *J. Power Sources* **1997**, *68*, 533.
(20) Julien, C. *Solid State Ionics* **2003**, *157*, 57.
(21) Rosolen, J. M.; Decker, F. *J. Electrochem. Soc.* **1996**, *143*, 2417.
(22) Andersson, A. S.; Kalska, B.; Häggströ m, L.; Thomas, J. O. *Solid State Ionics* **2000**, *130*, 41.
(23) Luo, J. Y.; Wang, Y. G.; Xiang, H. M.; Xia, Y. Y. *Chem. Mater.* **2007**, *19*, 4791.
(24) Sinha, N. N.; Munichandraiah, N. *ACS Appl. Mater. Interfaces* **2009**, *12*, 1241.
(25) Dedryvore, R.; Maccario, M.; Corgennec, L.; Le-Cars, F.; Delmas, C.; Genbeau, D. *Chem. Mater.* **2008**, *20*, 7164.
(26) Merel, P.; Tabbal, M.; Chaker, M.; Moisa, S.; Margot, J. *Appl. Surf. Sci.* **1998**, *136*, 105.
(27) Luo, J. Y.; Wang, Y. G.; Xiang, H. M.; Xia, Y. Y. *Chem. Mater.* **2007**, *19*, 4791.
(28) Maier, J. *Nat. Mater.* **2005**, *4*, 805.
(29) Winter, M.; Brodd, R. J. *Chem. Rev.* **2004**, *104*, 4245.
(30) Yang, H.; Wu, X. L.; Cao, M. H.; Guo, Y. G. *J. Phys. Chem. C* **2009**, *113*, 3345.
(31) Wang, J.; Polleux, J.; Lim, J.; Dunn, B. *J. Phys. Chem. C* **2007**, *111*, 14925.
(32) Wu, X. L.; Jiang, L. Y.; Cao, F. F.; Guo, Y. G.; Wan, L. J. *Adv. Mater.* **2009**, *21*, 2710.
(33) Lu, J. B.; Tang, Z. L.; Zhang, Z. T.; Shen, W. *Mater. Res. Bull.* **2005**, *40*, 2039.
(34) Zhao, B.; Jiang, Y.; Zhang, H.; Tao, H.; Zhang, M.; Jiao, Z. *J. Power Sources* **2009**, *189*, 462.

AM100309W